



HAL
open science

Finite Volume and Finite Element Schemes for the Euler Equation in Cylindrical and Spherical Coordinates

Dante de Santis, Gianluca Geraci, Alberto Guardone

► **To cite this version:**

Dante de Santis, Gianluca Geraci, Alberto Guardone. Finite Volume and Finite Element Schemes for the Euler Equation in Cylindrical and Spherical Coordinates. *Journal of Computational and Applied Mathematics*, 2012, 10.1016/j.cam.2012.02.006 . hal-00730349

HAL Id: hal-00730349

<https://inria.hal.science/hal-00730349>

Submitted on 10 Sep 2012

HAL is a multi-disciplinary open access archive for the deposit and dissemination of scientific research documents, whether they are published or not. The documents may come from teaching and research institutions in France or abroad, or from public or private research centers.

L'archive ouverte pluridisciplinaire **HAL**, est destinée au dépôt et à la diffusion de documents scientifiques de niveau recherche, publiés ou non, émanant des établissements d'enseignement et de recherche français ou étrangers, des laboratoires publics ou privés.

Finite Volume and Finite Element Schemes for the Euler Equation in Cylindrical and Spherical Coordinates

D. De Santis^a, G. Geraci^a, A. Guardone^b

^a*INRIA Bordeaux Sud-Ouest, équipe-projet Bacchus Cours de la Libération, 33405 Talence, France*

^b*Dipartimento di Ingegneria Aerospaziale Politecnico di Milano Via La Masa 34, 20156 Milano, Italy*

Abstract

A numerical scheme is presented for the solution of the compressible Euler equations over unstructured grids in cylindrical and spherical coordinates. The proposed scheme is based on a mixed finite volume / finite element approach. Numerical simulations are presented for the explosion problem in two spatial dimensions in cylindrical and spherical coordinates, and the numerical results are compared with the one-dimensional simulations for cylindrically and spherically symmetric explosions.

Keywords: Compressible flows, Cylindrical/Spherical Coordinates, Explosion problem, Finite Element/Volume Methods

1. Introduction

Some gasdynamics problems exhibit such strong symmetries that could be more convenient to describe these problems in a curvilinear reference, i.e. cylindrical or spherical, rather than in a Cartesian one. These are, e.g., astrophysical flows, Inertial Confinement Fusion (ICF) applications, sonoluminescence phenomena and nuclear explosions [1].

To compute the numerical solution of the compressible flow equations for these kind of flows, an interesting possibility is provided by the use of a mixed finite volume (FV) / finite element (FE) approach [2]. For example, in viscous flows, it is possible to use the FV and the FE to compute the advection and dissipation terms, respectively, within the same algorithm. Such a possibility is expected to be of use in the study of the effect of viscosity on e.g. the formation of stable shock fronts and on the determination of the onset and dynamics of Richtmyer-Meshkov instabilities in cylindrical and spherical implosions [3].

The combined use of these two different techniques is made possible by the introduction of suitable equivalence conditions that relate the FV metrics, i.e. cell volumes and integrated normals, to the FE integrals. Equivalence conditions relating FV and FE schemes have been derived for Cartesian coordinates in two and three spatial dimensions [4, 5] and for cylindrical coordinates in axially symmetric two-dimensional problems [6]. In both cited references, equivalence conditions are obtained by neglecting higher order FE contributions. Subsequently in [7], equivalence conditions for the cylindrical coordinates have been derived for the first time without introducing any approximation into the FE discrete expression of the divergence operator, and in [8] the differences between the consistent scheme and an alternative one violating the the equivalence conditions have been quantified for the case of one-dimensional problems in cylindrical and spherical coordinates. In the present paper the consistent formulation is presented in the cylindrical and spherical reference systems. Numerical results for the implosion and the explosion problem are also provided to demonstrate the correctness of the proposed approach.

The present paper is structured as follows. In section 2, the scalar equations in cylindrical and spherical coordinates are introduced. In sections 3 and 4 the spatial discretizations of the scalar equation by FE and FV are presented in

Email addresses: dante.de_santis@inria.fr (D. De Santis), gianluca.geraci@inria.fr (G. Geraci), alberto.guardone@polimi.it (A. Guardone)

cylindrical and spherical coordinates respectively. Equivalence conditions between FE and FV metrics are also shown. In section 6, numerical simulations are presented for the implosion and the explosion problem in the cylindrical coordinates on the R - θ and Z - R (axisymmetric) planes and in the spherical coordinates on the r - ϕ plane. Numerical results are also compared to one-dimensional simulations. In section 7 final remarks and comments are given.

2. Scalar equation in cylindrical and spherical coordinates

For simplicity we consider first a multidimensional scalar conservation law. The model equation in a three-dimensional cylindrical reference reads

$$\frac{\partial u}{\partial t} + \frac{\partial f_Z}{\partial Z} + \frac{1}{R} \frac{\partial}{\partial R}(R f_R) + \frac{1}{R} \frac{\partial f_\theta}{\partial \theta} = 0, \quad (1)$$

where t is the time, Z, R and θ are the axial, radial and azimuthal coordinates, respectively, $u = u(Z, R, \theta, t)$ is the scalar unknown and $\mathbf{f}^\circledast(u) = (f_Z, f_R, f_\theta)$ is the so-called flux function. A more compact form of the above equation is obtained by introducing the divergence operator in three-dimensional cylindrical coordinates $\nabla^\circledast \cdot (\cdot)$ as follows

$$\frac{\partial(u)}{\partial t} + \nabla^\circledast \cdot \mathbf{f}^\circledast(u) = 0. \quad (2)$$

The model equation in a three-dimensional spherical reference reads

$$\frac{\partial u}{\partial t} + \frac{1}{r^2} \frac{\partial}{\partial r}(r^2 f_r) + \frac{1}{r \sin \theta} \frac{\partial}{\partial \theta}(\sin \theta f_\theta) + \frac{1}{r \sin \theta} \frac{\partial f_\phi}{\partial \phi} = 0,$$

where r, θ and ϕ are the radial, polar and azimuthal coordinates, respectively, $u = u(r, \theta, \phi, t)$ is the scalar unknown and $\mathbf{f}^\circledast(u) = (f_r, f_\theta, f_\phi)$ is the flux function. In a compact form, using the divergence operator in three-dimensional spherical coordinates $\nabla^\circledast \cdot (\cdot)$, it can be rearranged as

$$\frac{\partial(u)}{\partial t} + \nabla^\circledast \cdot \mathbf{f}^\circledast(u) = 0. \quad (3)$$

3. Finite Volume/Element in cylindrical coordinates

3.1. Node-pair finite element discretization

The scalar conservation law (2) is now written in a weak form by multiplying it by the radial coordinate R and by a suitable Lagrangian test function $\phi_i \in V_h \subset H^1(\Omega)$. Integrating over the support Ω_i of ϕ_i gives

$$\int_{\Omega_i} R \phi_i \frac{\partial u}{\partial t} d\Omega_i + \int_{\Omega_i} R \phi_i \nabla^\circledast \cdot \mathbf{f}^\circledast(u) d\Omega_i = 0, \quad \forall i \in \mathcal{N}, \quad (4)$$

where \mathcal{N} is the set of all nodes of the triangulation. Note that by multiplying by R , the numerical singularity of the cylindrical reference system is formally removed [6]. In the following, to simplify the notation, the infinitesimal volume $d\Omega = R dR d\theta dZ$ is not indicated in the integrals. Integrating by parts immediately gives

$$\int_{\Omega_i} R \phi_i \frac{\partial u}{\partial t} = \int_{\Omega_i} R \mathbf{f}^\circledast \cdot \nabla^\circledast \phi_i + \int_{\Omega_i} \phi_i \mathbf{f}^\circledast \cdot \nabla^\circledast R - \int_{\partial\Omega_i^\circledast} R \phi_i \mathbf{f}^\circledast \cdot \mathbf{n}_i^\circledast \quad (5)$$

where $\partial\Omega_i^\circledast = \partial\Omega_i \cap \partial\Omega$, with $\partial\Omega_i$ and $\partial\Omega$ are the boundary of Ω_i and of the computational domain Ω , respectively, and where $\mathbf{n}_i^\circledast = n_Z \hat{\mathbf{Z}} + n_R \hat{\mathbf{R}} + n_\theta \hat{\boldsymbol{\theta}}$ is the outward normal versor to Ω_i . The scalar unknown is now interpolated as

$$u(Z, R, \theta, t) \simeq u_h(Z, R, \theta, t) = \sum_{k \in \mathcal{N}} u_k(t) \phi_k(Z, R, \theta),$$

to obtain the Bubnov-Galerkin approximation of the (1), namely

$$\sum_{k \in \mathcal{N}_i} \frac{du_k}{dt} M_{ik}^\circ = \int_{\Omega_i} R f^\circ(u_h) \cdot \nabla^\circ \varphi_i + \int_{\Omega_i} \varphi_i f^\circ(u_h) \cdot \nabla^\circ R - \int_{\partial \Omega_i^\circ} R \varphi_i f^\circ(u_h) \cdot \mathbf{n}^\circ, \quad (6)$$

where \mathcal{N}_i is the set of shape functions φ_k whose support Ω_k overlaps Ω_i of φ_i and where

$$M_{ik}^\circ \stackrel{\text{def}}{=} \int_{\Omega_{ik}} R \varphi_i \varphi_k d\Omega^\circ,$$

with $\Omega_{ik} = \Omega_i \cap \Omega_k$. By resorting the so-called flux interpolation technique [9], the flux function $f^\circ(u_h)$ is now expanded using the same shape function $\varphi_h \in V_h$ as follows

$$f^\circ(u_h) = f^\circ \left(\sum_{k \in \mathcal{N}} u_k(t) \varphi_k(Z, R, \theta) \right) \simeq \sum_{k \in \mathcal{N}} f_k^\circ(t) \varphi_k(Z, R, \theta),$$

where $f_k^\circ(t) = f^\circ(u_k(t))$, to obtain

$$\sum_{k \in \mathcal{N}_i} M_{ik}^\circ \frac{du_k}{dt} = \sum_{k \in \mathcal{N}_i} f_k^\circ(t) \cdot \left[\int_{\Omega_{ik}} R \varphi_k \nabla^\circ \varphi_i + \int_{\Omega_{ik}} \varphi_i \varphi_k \nabla^\circ R \right] - \sum_{k \in \mathcal{N}_i^\circ} f_k^\circ(t) \cdot \int_{\partial \Omega_{ik}^\circ} R \varphi_i \varphi_k \mathbf{n}_i^\circ,$$

where $\partial \Omega_{ik}^\circ = \partial \Omega_i \cap \partial \Omega_k \cap \partial \Omega$ and \mathcal{N}_i° is the set of all boundary nodes of Ω_i . Using the following identities

$$\begin{aligned} \sum_{k \in \mathcal{N}_i} f_k^\circ \cdot \int_{\Omega_{ik}} R \varphi_k \nabla^\circ \varphi_i &= \sum_{k \in \mathcal{N}_{i,\neq}} \left(\frac{f_k^\circ + f_i^\circ}{2} \cdot \boldsymbol{\eta}_{ik}^\circ - \frac{f_k^\circ - f_i^\circ}{2} \cdot \boldsymbol{\zeta}_{ik}^\circ \right) + \sum_{k \in \mathcal{N}_{i,\neq}} \frac{f_k^\circ - f_i^\circ}{2} \cdot \boldsymbol{\chi}_{ik}^\circ, \\ \sum_{k \in \mathcal{N}_i} f_k^\circ \cdot \int_{\partial \Omega_{ik}^\circ} R \varphi_i \varphi_k \mathbf{n}^\circ &= \sum_{k \in \mathcal{N}_{i,\neq}^\circ} (f_k^\circ - f_i^\circ) \cdot \boldsymbol{\chi}_{ik}^\circ - f_i^\circ \cdot \boldsymbol{\xi}_i^\circ, \end{aligned}$$

demonstrated in Appendix A, the node-pair representation of (6) is find to be

$$\begin{aligned} \sum_{k \in \mathcal{N}_i} M_{ik}^\circ \frac{du_k}{dt} &= - \sum_{k \in \mathcal{N}_{i,\neq}} \left(\frac{f_k^\circ + f_i^\circ}{2} \cdot \boldsymbol{\eta}_{ik}^\circ - \frac{f_k^\circ - f_i^\circ}{2} \cdot \boldsymbol{\zeta}_{ik}^\circ \right) \\ &\quad + f_i^\circ \cdot \widehat{\boldsymbol{\Gamma}}_i^\circ - \sum_{k \in \mathcal{N}_{i,\neq}^\circ} \frac{f_k^\circ - f_i^\circ}{2} \cdot \boldsymbol{\chi}_{ik}^\circ - f_i^\circ \cdot \boldsymbol{\xi}_i^\circ, \end{aligned} \quad (7)$$

where $\mathcal{N}_{i,\neq} = \mathcal{N}_i \setminus \{i\}$ and $\mathcal{N}_{i,\neq}^\circ = \mathcal{N}_i^\circ \setminus \{i\}$, and the following FE metric quantities have been introduced

$$\begin{aligned} \boldsymbol{\eta}_{ik}^\circ &\stackrel{\text{def}}{=} \int_{\Omega_{ik}} R (\varphi_i \nabla^\circ \varphi_k - \varphi_k \nabla^\circ \varphi_i), \\ \boldsymbol{\zeta}_{ik}^\circ &\stackrel{\text{def}}{=} \int_{\Omega_{ik}} \varphi_i \varphi_k \hat{\mathbf{R}}, \\ \widehat{\boldsymbol{\Gamma}}_i^\circ &\stackrel{\text{def}}{=} \sum_{k \in \mathcal{N}_i} \int_{\Omega_{ik}} \varphi_i \varphi_k \hat{\mathbf{R}} = \int_{\Omega_i} \varphi_i \hat{\mathbf{R}}, \\ \boldsymbol{\chi}_{ik}^\circ &\stackrel{\text{def}}{=} \int_{\partial \Omega_{ik}^\circ} R \varphi_i \varphi_k \mathbf{n}^\circ \quad \text{and} \quad \boldsymbol{\xi}_i^\circ \stackrel{\text{def}}{=} \int_{\partial \Omega_i^\circ} R \varphi_i \mathbf{n}^\circ. \end{aligned}$$

In the next section, the corresponding FV metrics are derived.

3.2. Edge-based finite volume discretization

The spatially discrete form of the scalar conservation law (2) is now obtained according to the node-centred finite volume approach [10]. To this purpose, the integral form of (2) times the radial coordinate R is enforced over a finite number of non-overlapping finite volumes C_i , with boundary ∂C_i . Over each control volume C_i the cell-averaged unknown is introduced as follows

$$u(Z, R, \theta, t) \simeq u_i(t) = \frac{1}{V_i} \int_{C_i} u(Z, R, \theta, t),$$

where V_i is the volume of the i -th cell. Splitting the boundary integral into interface and edge contributions

$$V_i^\varnothing \frac{du_i}{dt} = - \sum_{k \in \mathcal{N}_{i,\neq}} \int_{\partial C_{ik}} R \mathbf{f}^\varnothing \cdot \mathbf{n}_i^\varnothing - \int_{\partial C_i^\varnothing} R \mathbf{f}^\varnothing \cdot \mathbf{n}_i^\varnothing + \int_{C_i} \mathbf{f}^\varnothing \cdot \hat{\mathbf{R}}, \quad (8)$$

where $\mathcal{N}_{i,\neq}$ is the set of the finite volume C_k sharing a boundary with C_i , excluding C_i and where $\partial C_{ik} = \partial C_i \cap \partial C_k \neq \emptyset, k \neq i$, is the so-called cell interface. As it is standard practice, the flux vector is assumed to be constant over each cell interface. Under this assumption, the domain and boundary contributions read

$$\begin{aligned} \int_{\partial C_{ik}} R \mathbf{f}^\varnothing \cdot \mathbf{n}_i^\varnothing &\simeq \mathbf{f}_{ik}^\varnothing \cdot \int_{\partial C_{ik}} R \mathbf{n}_i^\varnothing = \mathbf{f}_{ik}^\varnothing \cdot \mathbf{v}_{ik}^\varnothing & \text{with} & \quad \mathbf{v}_{ik}^\varnothing \stackrel{\text{def}}{=} \int_{\partial C_{ik}} R \mathbf{n}_i^\varnothing & \text{and} \\ \int_{\partial C_i^\varnothing} R \mathbf{f}^\varnothing \cdot \mathbf{n}_i^\varnothing &\simeq \mathbf{f}_i^\varnothing \cdot \int_{\partial C_i^\varnothing} R \mathbf{n}_i^\varnothing = \mathbf{f}_i^\varnothing \cdot \mathbf{v}_i^\varnothing & \text{with} & \quad \mathbf{v}_i^\varnothing \stackrel{\text{def}}{=} \int_{\partial C_i^\varnothing} R \mathbf{n}_i^\varnothing, \end{aligned}$$

respectively. If a second-order centred approximation of the fluxes is considered, namely, $\mathbf{f}_{ik}^\varnothing = (\mathbf{f}_i^\varnothing + \mathbf{f}_k^\varnothing)/2$, the final form of the finite volume approximation of (2) reads,

$$V_i^\varnothing \frac{du_i}{dt} = - \sum_{k \in \mathcal{N}_{i,\neq}} \frac{\mathbf{f}_i^\varnothing + \mathbf{f}_k^\varnothing}{2} \cdot \mathbf{v}_{ik}^\varnothing + \mathbf{f}_i^\varnothing \cdot \widehat{\mathbf{v}}_i^\varnothing - \mathbf{f}_i^\varnothing \cdot \mathbf{v}_i^\varnothing \quad \text{with} \quad \widehat{\mathbf{v}}_i^\varnothing \stackrel{\text{def}}{=} \int_{C_i} \hat{\mathbf{R}}, \quad (9)$$

to be compared with the corresponding FE discretization (7).

3.3. Finite Element/Volume equivalence

The equivalence conditions relating the above FV metric quantities and the FE ones defined in the previous section are now derived. To this purpose, relevant properties of the FE and FV discretizations are briefly recalled.

Considering FE metric quantities first, from its definition the vector $\boldsymbol{\eta}_{ik}^\varnothing$ is asymmetric, namely, $\boldsymbol{\eta}_{ik}^\varnothing = -\boldsymbol{\eta}_{ki}^\varnothing$ which will be referred in the following as property FEM-a. Property FEM-b is obtained by noting that $\sum_{k \in \mathcal{N}_i} (\boldsymbol{\eta}_{ik}^\varnothing - \boldsymbol{\zeta}_{ik}^\varnothing) + \boldsymbol{\xi}_i^\varnothing = \mathbf{0}$ which gives immediately

$$\widehat{\mathbf{L}}_i^\varnothing = \sum_{k \in \mathcal{N}_{i,\neq}} \boldsymbol{\eta}_{ik}^\varnothing + \boldsymbol{\xi}_i^\varnothing. \quad (10)$$

Property FEM-c stems from the following identity

$$3L_i^\varnothing = \int_{\Omega_i} R \varphi_i \nabla^\varnothing \cdot \mathbf{x}^\varnothing = \int_{\partial \Omega_i^\varnothing} R \varphi_i \mathbf{x}^\varnothing \cdot \mathbf{n}_i^\varnothing - \int_{\Omega_i} \varphi_i \mathbf{x}^\varnothing \cdot \hat{\mathbf{R}} - \int_{\Omega_i} R \mathbf{x}^\varnothing \cdot \nabla^\varnothing \varphi_i, \quad (11)$$

where \mathbf{x}^\varnothing is the position vector, $\mathbf{x}^\varnothing = Z\hat{\mathbf{Z}} + R\hat{\mathbf{R}}(\theta)$. By substituting the exact expansion $\mathbf{x}^\varnothing = \sum_{k \in \mathcal{N}_i} \mathbf{x}_k^\varnothing \varphi_k$, and applying node-pair representation described in the subsection 4.1, Eq. (11) can be written as

$$3L_i^\varnothing = \sum_{k \in \mathcal{N}_{i,\neq}} \left[\frac{\mathbf{x}_k^\varnothing + \mathbf{x}_i^\varnothing}{2} \cdot \boldsymbol{\eta}_{ik}^\varnothing - \frac{\mathbf{x}_k^\varnothing - \mathbf{x}_i^\varnothing}{2} \cdot \boldsymbol{\zeta}_{ik}^\varnothing \right] - \widehat{\mathbf{L}}_i^\varnothing \cdot \mathbf{x}_i^\varnothing + \sum_{k \in \mathcal{N}_{i,\neq}} \frac{\mathbf{x}_k^\varnothing - \mathbf{x}_i^\varnothing}{2} \cdot \boldsymbol{\chi}_{ik}^\varnothing + \mathbf{x}_i^\varnothing \cdot \boldsymbol{\xi}_i^\varnothing.$$

By substituting property FEM-b in the above identity, one finally obtain property FEM-c as

$$3L_i^\varnothing = \sum_{k \in \mathcal{N}_{i,\neq}} \left[\frac{\mathbf{x}_k^\varnothing + \mathbf{x}_i^\varnothing}{2} \cdot \boldsymbol{\eta}_{ik}^\varnothing - \frac{\mathbf{x}_k^\varnothing - \mathbf{x}_i^\varnothing}{2} \cdot \boldsymbol{\zeta}_{ik}^\varnothing \right] + \sum_{k \in \mathcal{N}_{i,\neq}} \frac{\mathbf{x}_k^\varnothing - \mathbf{x}_i^\varnothing}{2} \cdot \boldsymbol{\chi}_{ik}^\varnothing. \quad (12)$$

Considering now FV metric quantities, from the fact that $\mathbf{n}_i^\circ = -\mathbf{n}_k^\circ$ over ∂C_{ik} , property FVM-a reads $\mathbf{v}_{ik}^\circ = -\mathbf{v}_{ki}^\circ$, which corresponds to the conservation property of the scheme. From the Gauss theorem, one also has

$$\int_{C_i} \nabla^\circ R = \oint_{\partial C_i} R \mathbf{n}_i^\circ,$$

which, from the definition of FV metric quantities, gives property FVM-b as

$$\widehat{\mathbf{V}}_i^\circ = \sum_{k \in \mathcal{N}_{i,\neq}} \mathbf{v}_{ik}^\circ + \mathbf{v}_i^\circ. \quad (13)$$

Property FVM-c is obtained by noting that

$$3V_i^\circ = \int_{C_i} R \nabla^\circ \cdot \mathbf{x}^\circ = \oint_{\partial C_i} R \mathbf{x}^\circ \cdot \mathbf{n}_i^\circ - \int_{C_i} \widehat{\mathbf{R}} \cdot \mathbf{x}^\circ. \quad (14)$$

The right hand side of (14) is now computed by means of the FV discretization described in subsection 3.2 as

$$3V_i^\circ = \sum_{k \in \mathcal{N}_{i,\neq}} \frac{\mathbf{x}_k^\circ + \mathbf{x}_i^\circ}{2} \cdot \mathbf{v}_{ik}^\circ - \mathbf{x}_i^\circ \cdot \widehat{\mathbf{L}}_i^\circ + \mathbf{x}_i^\circ \cdot \mathbf{v}_i^\circ.$$

which from property FVM-b becomes

$$3V_i^\circ = \sum_{k \in \mathcal{N}_{i,\neq}} \frac{\mathbf{x}_k^\circ + \mathbf{x}_i^\circ}{2} \cdot \mathbf{v}_{ik}^\circ. \quad (15)$$

Therefore, a FV approximation can be formally obtained from FE metric quantities defined over the same grid points by setting (see properties FEM/FVM-a and -b)

$$\mathbf{v}_{ik}^\circ = \boldsymbol{\eta}_{ik}^\circ, \quad \mathbf{v}_i^\circ = \boldsymbol{\xi}_i^\circ, \quad \widehat{\mathbf{V}}_i^\circ = \widehat{\mathbf{L}}_i^\circ.$$

Note that the mass lumping approximation,

$$\sum_{k \in \mathcal{N}_i} M_{ik}^\circ \frac{du_k}{dt} \simeq L_i^\circ \frac{du_i}{dt}$$

has to be introduced in the Eq. (7) for the equivalence conditions to be applicable. By subtracting Eq. (12) to Eq. (15), one finally has

$$V_i^\circ = L_i^\circ + \sum_{k \in \mathcal{N}_{i,\neq}} \frac{\mathbf{x}_k^\circ - \mathbf{x}_i^\circ}{6} \cdot \boldsymbol{\zeta}_{ik}^\circ - \sum_{k \in \mathcal{N}_{i,\neq}^\theta} \frac{\mathbf{x}_k^\circ - \mathbf{x}_i^\circ}{6} \cdot \boldsymbol{\chi}_{ik}^\circ. \quad (16)$$

It is remarkable that, differently from the Cartesian case [4, 5], in the cylindrical reference the FV cell is not coincident with the FE lumped mass matrix. Moreover, the shape of the FV cells that guarantees equivalence with FE discretization still remains to be determined.

4. Finite Volume/Element method in spherical coordinates

4.1. Node-pair finite element discretization

In the present section the spatial discretization of conservation law in a spherical reference system is presented.

The scalar conservation law (3) is multiplied by the quantity $r \sin \theta$ to formally remove the singularity of the spherical coordinate system along the zenith direction. The FE node-pair discretization is obtained as done in the cylindrical case [11], namely

$$M_{ik}^\circ \frac{du_i}{dt} = - \sum_{k \in \mathcal{N}_{i,\neq}} \left(\frac{\mathbf{f}_k^\circ + \mathbf{f}_i^\circ}{2} \cdot \boldsymbol{\eta}_{ik}^\circ - \frac{\mathbf{f}_k^\circ - \mathbf{f}_i^\circ}{2} \cdot \boldsymbol{\zeta}_{ik}^\circ \right) + \mathbf{f}_i^\circ \cdot \widehat{\mathbf{L}}_i^\circ - \sum_{k \in \mathcal{N}_{i,\neq}^\theta} \frac{\mathbf{f}_k^\circ - \mathbf{f}_i^\circ}{2} \cdot \boldsymbol{\chi}_{ik}^\circ - \mathbf{f}_i^\circ \cdot \boldsymbol{\xi}_i^\circ, \quad (17)$$

where the following metric quantities have been introduced

$$\begin{aligned}
M_{ik}^\circ &\stackrel{\text{def}}{=} \int_{\Omega_{ik}} r \sin \theta \varphi_i \varphi_k d\Omega^\circ, & \eta_{ik}^\circ &\stackrel{\text{def}}{=} \int_{\Omega_{ik}} r \sin \theta (\varphi_i \nabla^\circ \varphi_k - \varphi_k \nabla^\circ \varphi_i) d\Omega^\circ, \\
\zeta_{ik}^\circ &\stackrel{\text{def}}{=} \int_{\Omega_{ik}} \varphi_i \varphi_k \nabla^\circ (r \sin \theta) d\Omega^\circ, & \widehat{L}_i^\circ &\stackrel{\text{def}}{=} \sum_{k \in N_{i,\neq}} \int_{\Omega_{ik}} \varphi_i \varphi_k \nabla^\circ (r \sin \theta) d\Omega^\circ, \\
\chi_{ik}^\circ &\stackrel{\text{def}}{=} \int_{\partial\Omega_{ik}^\circ} r \sin \theta \varphi_i \varphi_k \mathbf{n}^\circ d\partial\Omega^\circ, & \xi_i^\circ &\stackrel{\text{def}}{=} \int_{\partial\Omega_{ik}^\circ} r \sin \theta \varphi_i \mathbf{n}^\circ d\partial\Omega^\circ.
\end{aligned}$$

4.2. Edge-based finite volume discretization

The FV spatially discrete form of the scalar conservation law (3) multiplied by the quantity $r \sin \theta$ reads

$$V_i^\circ \frac{du_i}{dt} = - \sum_{k \in N_{i,\neq}} \frac{f_i^\circ + f_k^\circ}{2} \cdot \mathbf{v}_{ik}^\circ + f_i^\circ \cdot \widehat{\mathbf{V}}_i^\circ - f_i^\circ \cdot \mathbf{v}_i^\circ \quad (18)$$

where

$$\widehat{\mathbf{V}}_i^\circ \stackrel{\text{def}}{=} \int_{\partial\mathcal{C}_i^\circ} \nabla^\circ (r \sin \theta), \quad \mathbf{v}_{ik}^\circ \stackrel{\text{def}}{=} \int_{\partial\mathcal{C}_{ik}^\circ} r \sin \theta \mathbf{n}_i^\circ \quad \text{and} \quad \mathbf{v}_i^\circ \stackrel{\text{def}}{=} \int_{\partial\mathcal{C}_i^\circ} r \sin \theta \mathbf{n}_i^\circ$$

4.3. Finite Element/Volume equivalence

The equivalence conditions relating the FV and FE scheme are obtained like in the cylindrical case. The following properties are introduced for the FE metric quantities

$$\begin{aligned}
(\text{FEM} - \text{a}) \quad \eta_{ik}^\circ &= -\eta_{ki}^\circ & (19) \\
(\text{FEM} - \text{b}) \quad \widehat{L}_i^\circ &= \sum_{k \in N_{i,\neq}} \eta_{ik}^\circ + \xi_i^\circ \\
(\text{FEM} - \text{c}) \quad 3L_i^\circ &= \int_{\partial\Omega_i^\circ} r \sin \theta \varphi_i \mathbf{x}^\circ \cdot \mathbf{n}_i^\circ - \int_{\Omega_i^\circ} \varphi_i \mathbf{x}^\circ \cdot \hat{\mathbf{r}} - \int_{\Omega_i^\circ} r \sin \theta \mathbf{x}^\circ \cdot \nabla^\circ \varphi_i
\end{aligned}$$

and for the FV metric quantities

$$\begin{aligned}
(\text{FVM} - \text{a}) \quad \mathbf{n}_i^\circ &= -\mathbf{n}_k^\circ & (20) \\
(\text{FVM} - \text{b}) \quad \widehat{\mathbf{V}}_i^\circ &= \sum_{k \in N_{i,\neq}} \mathbf{v}_{ik}^\circ + \mathbf{v}_i^\circ \\
(\text{FVM} - \text{c}) \quad 3V_i^\circ &= \sum_{k \in N_{i,\neq}} \frac{\mathbf{x}_i^\circ + \mathbf{x}_k^\circ}{2} \cdot \mathbf{v}_{ik}^\circ
\end{aligned}$$

Therefore, a FV approximation can be formally obtained from FE metric quantities defined over the same grid points by setting (see properties FEM/FVM-a and -b)

$$\mathbf{v}_{ik}^\circ = \eta_{ik}^\circ, \quad \mathbf{v}_i^\circ = \xi_i^\circ, \quad \widehat{\mathbf{V}}_i^\circ = \widehat{L}_i^\circ.$$

By subtracting (FEM-c) to (FVM-c), one finally has

$$V_i^\circ = L_i^\circ + \sum_{k \in N_{i,\neq}} \frac{\mathbf{x}_k^\circ - \mathbf{x}_i^\circ}{6} \cdot \zeta_{ik}^\circ - \sum_{k \in N_{i,\neq}} \frac{\mathbf{x}_k^\circ - \mathbf{x}_i^\circ}{6} \cdot \chi_{ik}^\circ, \quad (21)$$

where, like the cylindrical case, the mass lumping approximation has been introduced. It is clear that also in this case the FV cell is not coincident with the FE lumped mass matrix and the shape of the FV cells that guarantees equivalence with FE discretization still remains undetermined.

5. Fully discrete form of the Euler equations in cylindrical and spherical coordinates

The Euler equations in cylindrical and spherical coordinates for compressible inviscid flows are now briefly recalled. The differential form reads

$$\frac{\partial \mathbf{u}^\circ}{\partial t} + \nabla^\circ \cdot \mathbf{f}^\circ = \frac{1}{R} \mathbf{s}^\circ \quad \text{and} \quad \frac{\partial \mathbf{u}^\circ}{\partial t} + \nabla^\circ \cdot \mathbf{f}^\circ = \frac{1}{r \sin \theta} \mathbf{s}^\circ,$$

respectively, where $\mathbf{u}^\circ(Z, R, \theta, t) = (\rho, \mathbf{m}^\circ, E^t)^\top$ and $\mathbf{u}^\circ(r, \theta, \phi, t) = (\rho, \mathbf{m}^\circ, E^t)^\top$, with ρ density, $\mathbf{m}^\circ = (m_Z, m_R, m_\theta)^\top$, $\mathbf{m}^\circ = (m_r, m_\theta, m_\phi)^\top$ momentum and E^t total energy per unit volume. The flux function and the source term are defined as follow in the cylindrical case

$$\mathbf{f}^\circ = \begin{pmatrix} m_Z & m_R & m_\theta \\ \frac{m_Z^2}{\rho} + \Pi & \frac{m_R m_Z}{\rho} & \frac{m_\theta m_Z}{\rho} \\ \frac{m_Z m_R}{\rho} & \frac{m_R^2}{\rho} + \Pi & \frac{m_\theta m_R}{\rho} \\ \frac{m_Z m_\theta}{\rho} & \frac{m_R m_\theta}{\rho} & \frac{m_\theta^2}{\rho} + \Pi \\ \frac{m_Z}{\rho} (E^t + \Pi) & \frac{m_R}{\rho} (E^t + \Pi) & \frac{m_\theta}{\rho} (E^t + \Pi) \end{pmatrix}, \quad \mathbf{s}^\circ = \begin{pmatrix} 0 \\ 0 \\ \frac{m_\theta^2}{\rho} + \Pi \\ \frac{m_\theta m_R}{\rho} \\ 0 \end{pmatrix},$$

and in the spherical one

$$\mathbf{f}^\circ(\mathbf{u}^\circ) = \begin{pmatrix} m_r & m_\theta & m_\phi \\ \frac{m_r^2}{\rho} + \Pi & \frac{m_\theta m_r}{\rho} & \frac{m_\phi m_r}{\rho} \\ \frac{m_r m_\theta}{\rho} & \frac{m_\theta^2}{\rho} + \Pi & \frac{m_\phi m_\theta}{\rho} \\ \frac{m_r m_\phi}{\rho} & \frac{m_\theta m_\phi}{\rho} & \frac{m_\phi^2}{\rho} + \Pi \\ \frac{m_r}{\rho} (E^t + \Pi) & \frac{m_\theta}{\rho} (E^t + \Pi) & \frac{m_\phi}{\rho} (E^t + \Pi) \end{pmatrix},$$

$$\mathbf{s}^\circ(\mathbf{u}^\circ) = \begin{pmatrix} 0 \\ \left(\frac{m_\theta^2}{\rho} + \Pi \right) + \left(\frac{m_\phi^2}{\rho} + \Pi \right) \\ -\frac{m_\theta m_r}{\rho} \\ -\frac{m_\phi m_r}{\rho} \\ 0 \end{pmatrix} \sin \theta + \begin{pmatrix} 0 \\ 0 \\ \frac{m_\phi^2}{\rho} + \Pi \\ -\frac{m_\theta m_\phi}{\rho} \\ 0 \end{pmatrix} \cos \theta = \check{\mathbf{s}}^\circ \sin \theta + \bar{\mathbf{s}}^\circ \cos \theta.$$

where Π is the pressure function in terms of the conservative variables.

The FV spatially-discrete form of the Euler equations in the cylindrical and spherical references reads

$$V_i^\circ \frac{d\mathbf{u}_i^\circ}{dt} = - \sum_{k \in \mathcal{N}_i, \neq} \frac{\mathbf{f}_k^\circ + \mathbf{f}_i^\circ}{2} \cdot \boldsymbol{\eta}_{ik}^\circ + L_i s_i^\circ - \mathbf{f}_i^\circ \cdot \boldsymbol{\xi}_i^\circ \quad \text{and} \quad (22)$$

$$V_i^\circ \frac{d\mathbf{u}_i^\circ}{dt} = - \sum_{k \in \mathcal{N}_i, \neq} \frac{\mathbf{f}_i^\circ + \mathbf{f}_k^\circ}{2} \cdot \boldsymbol{\eta}_{ik}^\circ + \mathbf{f}_i^\circ \cdot \widehat{\mathcal{L}}_i^\circ - \mathbf{f}_i^\circ \cdot \boldsymbol{\xi}_i^\circ + \check{s}_i^\circ \hat{L}_i + \bar{s}_i^\circ \check{L}_i,$$

respectively, where the following notation has been used $s_i^\circ \stackrel{\text{def}}{=} s^\circ(\mathbf{u}_i^\circ)$, $\check{s}_i^\circ \stackrel{\text{def}}{=} \check{\mathbf{s}}^\circ(\mathbf{u}_i^\circ)$, $\bar{s}_i^\circ \stackrel{\text{def}}{=} \bar{\mathbf{s}}^\circ(\mathbf{u}_i^\circ)$. The terms V_i° and V_i° are computed from the equivalence condition in cylindrical and spherical case, respectively. In the computation,

a TVD [12] numerical flux is used, with the van Leer limiter [13]. The fully discrete form of the Euler system is obtained by a two-step Backward Differencing Formulæ. At each time level, a dual time-stepping technique is used to solve the time-implicit problem [14]. In all simulation the ideal gas model for the nitrogen ($\gamma = c_p/c_v = 1.39$) is used.

6. Numerical results

In the present section, numerical results for converging and diverging shock waves are presented for both the cylindrical and spherical cases.

The first problem consider is a one dimensional simulation of converging shocks in cylindrical and spherical symmetry. This kind of problems can be seen as a special Riemann problem in cylindrical and spherical coordinates for which Guderley [15] has showed that the position of the converging shock has a similar solution as follows

$$\frac{R}{R_c} = A^\pm \left(1 - \frac{t}{t_c}\right)^\alpha,$$

where $R = R(t)$ is the position of the shock as function of the time t , R_c is the position of the discontinuity at initial time and t_c is the time value at which the discontinuity reaches the origin of the domain. The rational number α is the exponent of the similar law and A^+ and A^- are the coefficients for the converging and diverging shock, respectively. All these coefficients can be computed in the case of the polytropic ideal gas [15].

The numerical simulation are performed on a one dimensional domain with wall boundary conditions at the two boundaries. The initial solution consists of a uniform distribution of the density, the velocity is zero everywhere, while the pressure has a discontinuity at the center of the domain with a value of the pressure on the outer part of the domain ten times higher that the value on the inner part.

In figure 1 the Guderley's law is compared against the numerical results on a grid of 501 ($\Delta r = 2 \times 10^{-3}$) nodes with a time step $\Delta t = 10^{-4}$ for both the cylindrical and spherical problems. The numerical and the analytical solutions agree very well, even near the origin of the domain where there are strong shocks. After the shocks reflections, there are complex interactions between the waves coming to the origin and those reflected that are not taken into account by the analytical model.

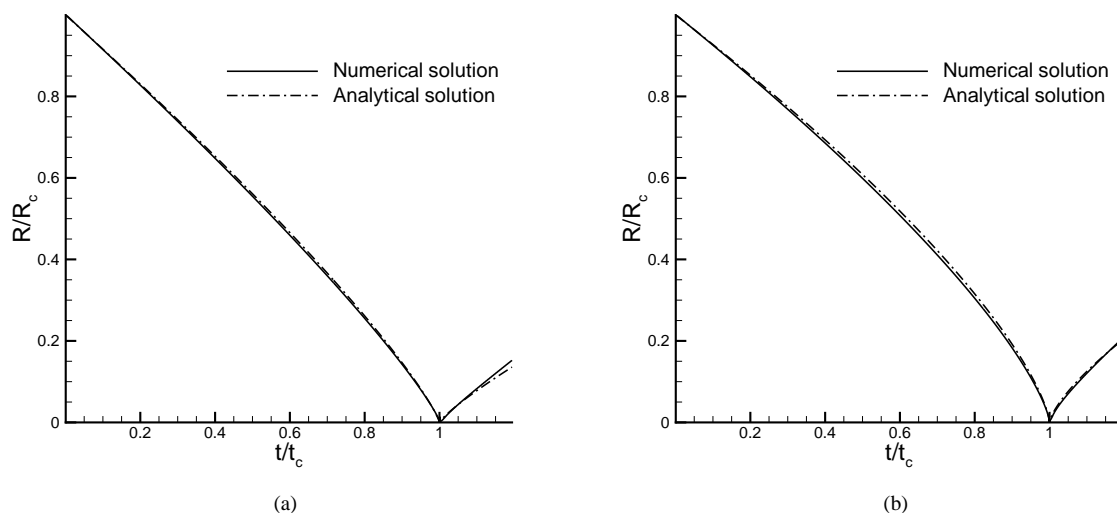


Figure 1: Position of the converging shock as function of the time for the one-dimensional simulation and for the analytical solution of Guderley: (a) cylindrical problem, (b) spherical problem.

The explosion and the implosion problem are now considered in the case of two spatial dimension. The computational domain is shown in figure 2, where a representative computational grid is also shown.

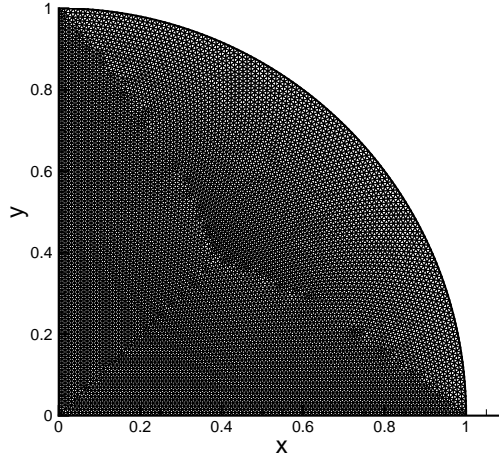


Figure 2: Exemplary grid for the explosion and implosion problems. The grid is the coarse grid.

Initial conditions for the explosion problem are as follows. The velocity is assumed to be zero everywhere; the density is uniform and equal to 1, whereas the pressure is uniform and equal to 10 in a circular region centered at the origin with radius $r = 0.5$. In the remaining portion of the domain, the pressure is uniform and equal to 1.

The thermodynamics variables are made dimensionless by the corresponding value at rest (outer region), the spatial dimensions are made dimensionless by the radius of the domain. Velocity and time are made dimensionless by the square root of the reference pressure divided by the reference density; the reference time is the reference length divided by the reference velocity.

In figure 3 and 4 are reported the numerical solution respectively for the cylindrical coordinates system on the plane $R-\theta$ and spherical coordinates on the plane $r-\phi$, for the explosion problem. The density isolines at different time levels are shown together with the pressure profiles along the axis $y = 0$. The grid is made with 39 153 nodes 77 587 triangles and the time step is 2.5×10^{-4} . A shock wave propagates towards the outer boundary of the computational domain; the shock wave is followed by a contact discontinuity. A rarefaction wave propagates towards the origin and is then reflected outward. Note that the initial corrugation of the shock front, due to the un-even shape of the initial discontinuity caused by its discrete representation over an unstructured grid of triangles, is clearly visible also at later times. The pressure profiles are compared against reference one-dimensional results for the three different time levels. One-dimensional computations were performed over a evenly-spaced grid made of 2 001 nodes, which corresponds to an element spacing of 5×10^{-4} .

A grid dependence study is shown in figure 5. Pressure signals along the $y = 0$ axis are compared at time $t = 0.16$ for three different grid resolutions: the coarse grid is made of 9 551 nodes and 18 745 triangles, the medium one is made of 20 683 nodes and 40 841 triangles, the fine one is made of 39 153 nodes 77 587 triangles. Numerical results are found to be almost independent from the grid resolution. Time step dependence can be appreciated from figure 6, where the pressure signals for three different time steps is shown at time $t = 0.16$ for the medium grid. Numerical results are found to be independent from the chosen time step.

In figure 7 and figure 8, numerical results for the implosion problem are showed in cylindrical and spherical case respectively. In the implosion problem the initial conditions are as in the explosion problem where now the high pressure region is the outer one and the low pressure region is at $r < 0.5$. The grid is the fine grid and the time step is 2.5×10^{-4} . A rarefaction wave propagates towards the outer boundary; a shock wave and a contact surface propagates inwards. The intensity of the shock increases as it moves towards the origin; when the shock wave is reflected at the origin, a region of high pressure/temperature is observed. In the spherical case, this effect is more evident.

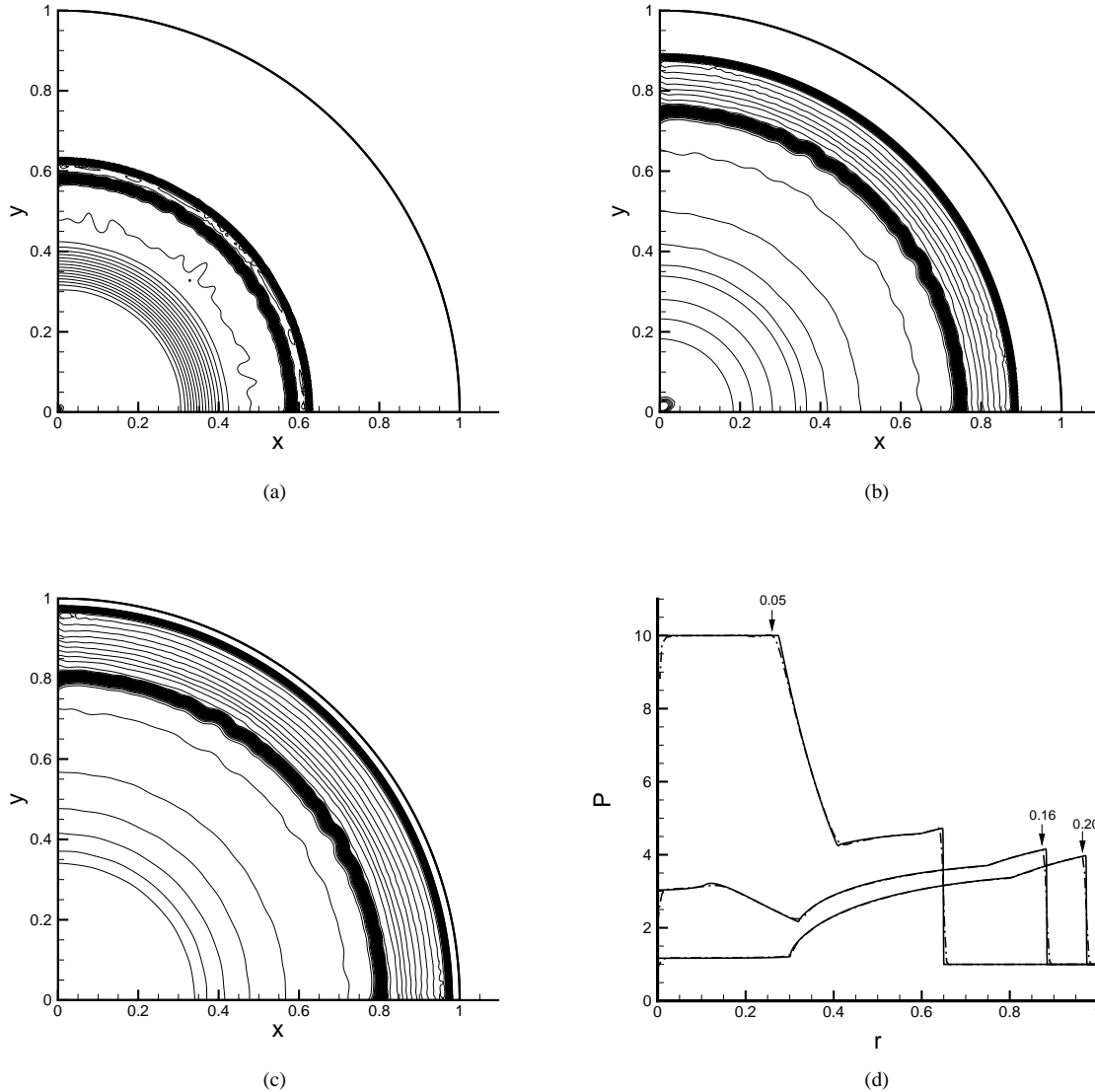


Figure 3: Density isoline for the cylindrical implosion problem: (a) $t = 0.02$; (b) $t = 0.12$; (c) $t = 0.16$. Each isoline corresponds to a density difference of $\Delta\rho/\rho_{ref} = 0.03$. (d) Pressure signal along the $y = 0$ axis at the same time levels: the solid line is the reference one-dimensional solutions, the dot-dashed line is the bidimensional solution.

Due to the symmetry of the solution and of the computational domain, the spherical implosion and explosion problems can be also simulated by axially symmetric Euler equations formulated in a cylindrical coordinate system, as done in [7]. The spherical and axisymmetric solution correspond to the solution of the same problem on two different planes, i.e., the r - ϕ plane in the spherical problem and the Z - R plane in the axisymmetric problem, where Z is the coordinate along the axis of symmetry and R is the coordinate along the axis normal to the axis of symmetry. The solutions in spherical coordinates are shown together with the corresponding solutions in axisymmetric coordinates in figure 9 for the implosion problem. In order to reconstruct the complete spherical solution the spherical and axisymmetric solutions are represented on each own plane.

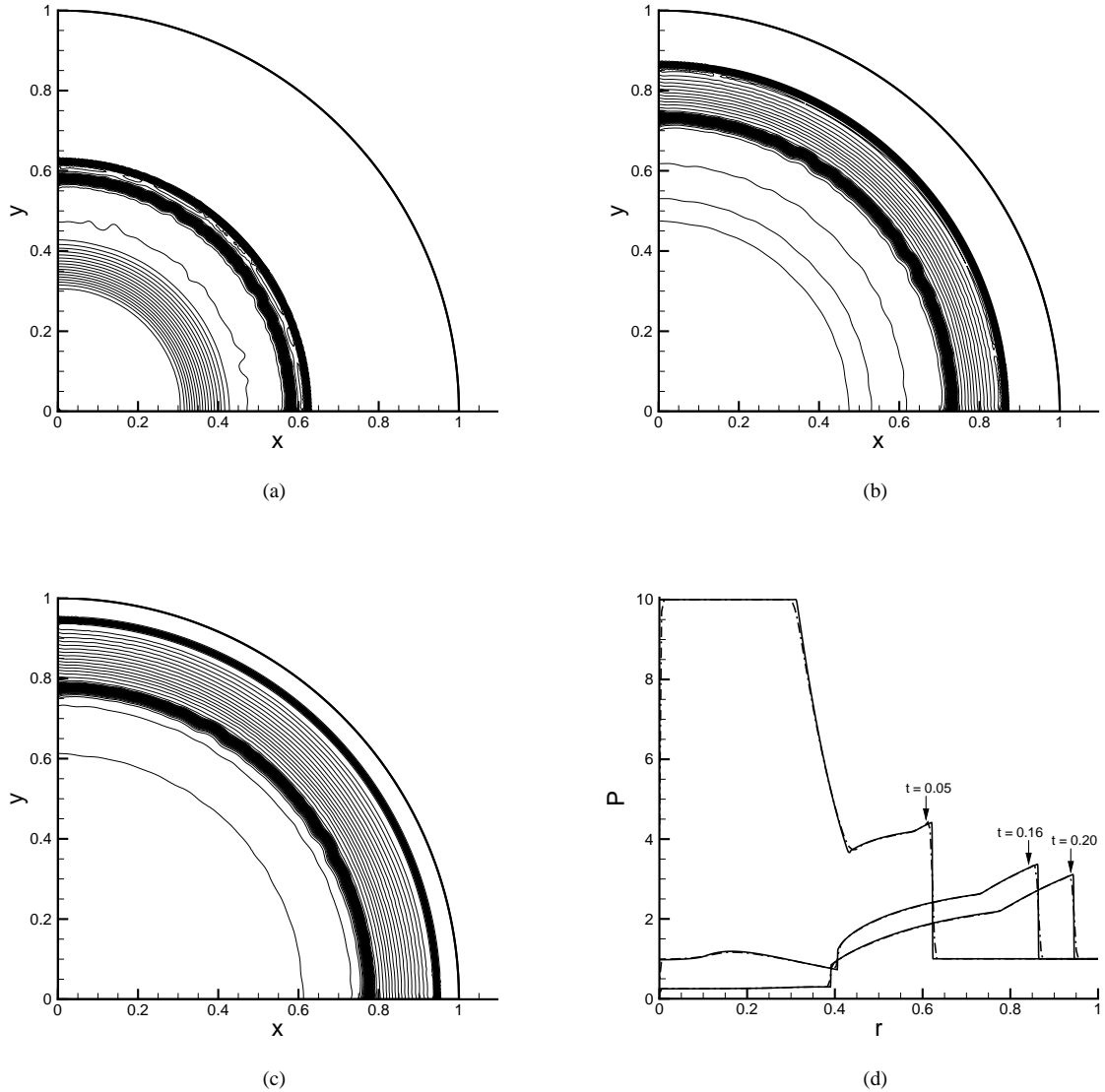


Figure 4: Density isoline for the spherical implosion problem: (a) $t = 0.02$; (b) $t = 0.12$; (c) $t = 0.16$. Each isoline corresponds to a density difference of $\Delta\rho/\rho_{ref} = 0.03$. (d) Pressure signal along the $y = 0$ axis at the same time levels: the solid line is the reference one-dimensional solutions, the dot-dashed line is the bidimensional solution.

7. Conclusions

A novel unstructured-grid hybrid finite element/volume method in a cylindrical and spherical reference was presented. The proposed approach represents an extension of the node-pair scheme earlier for the cartesian coordinates and moves from suitable equivalence conditions linking finite element integrals to the corresponding finite volume metrics, such as the cell volume or the integrated normals. The equivalence conditions, as done for the first time in the case for the cylindrical coordinates [7], were derived here without introducing any approximation and allowed to determine all needed finite volume metric quantities from finite element ones. Numerical results are presented for one and two spatial dimension compressible flows: these consist in the numerical simulation of the explosion and im-

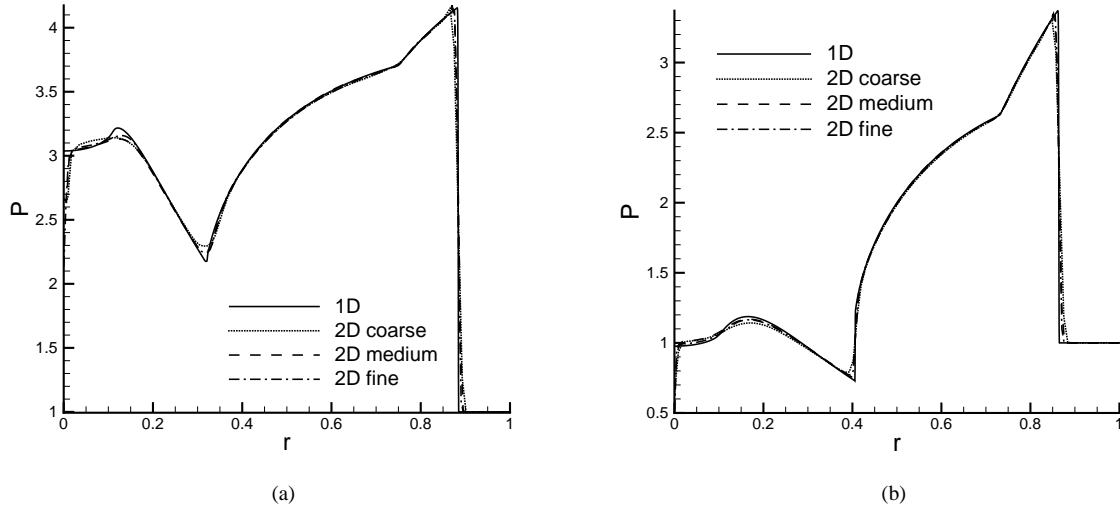


Figure 5: Comparison of pressure signals along the $y = 0$ axis for the explosion problem at time $t = 0.16$ for different grid resolutions against one dimensional simulations. Left: cylindrical case, right: spherical case.

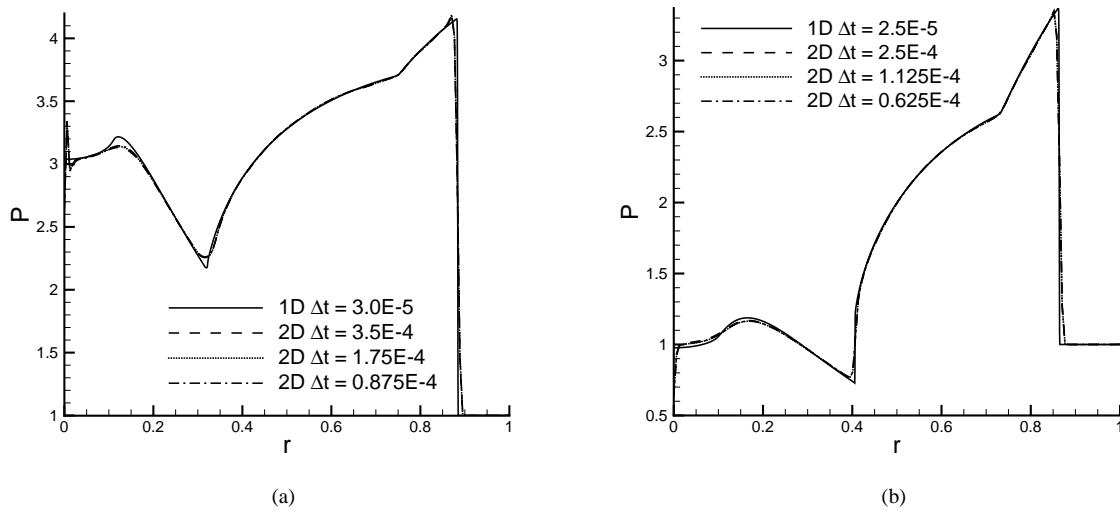


Figure 6: Comparison of pressure signals along the $y = 0$ axis for the explosion problem at time $t = 0.16$ for diverse time steps against one dimensional simulations. Left: cylindrical case, right: spherical case.

plosion problems, in which an initial discontinuity in pressure results in the formation of a diverging and converging shock, respectively. The computed pressure and density profile agree fairly well with one-dimensional simulation in cylindrical and spherical symmetry over a very fine grid. The solutions obtained in spherical reference also agree very well with the corresponding solutions in a cylindrical reference where the axisymmetric condition has been used to simulate spherical explosions and implosions.

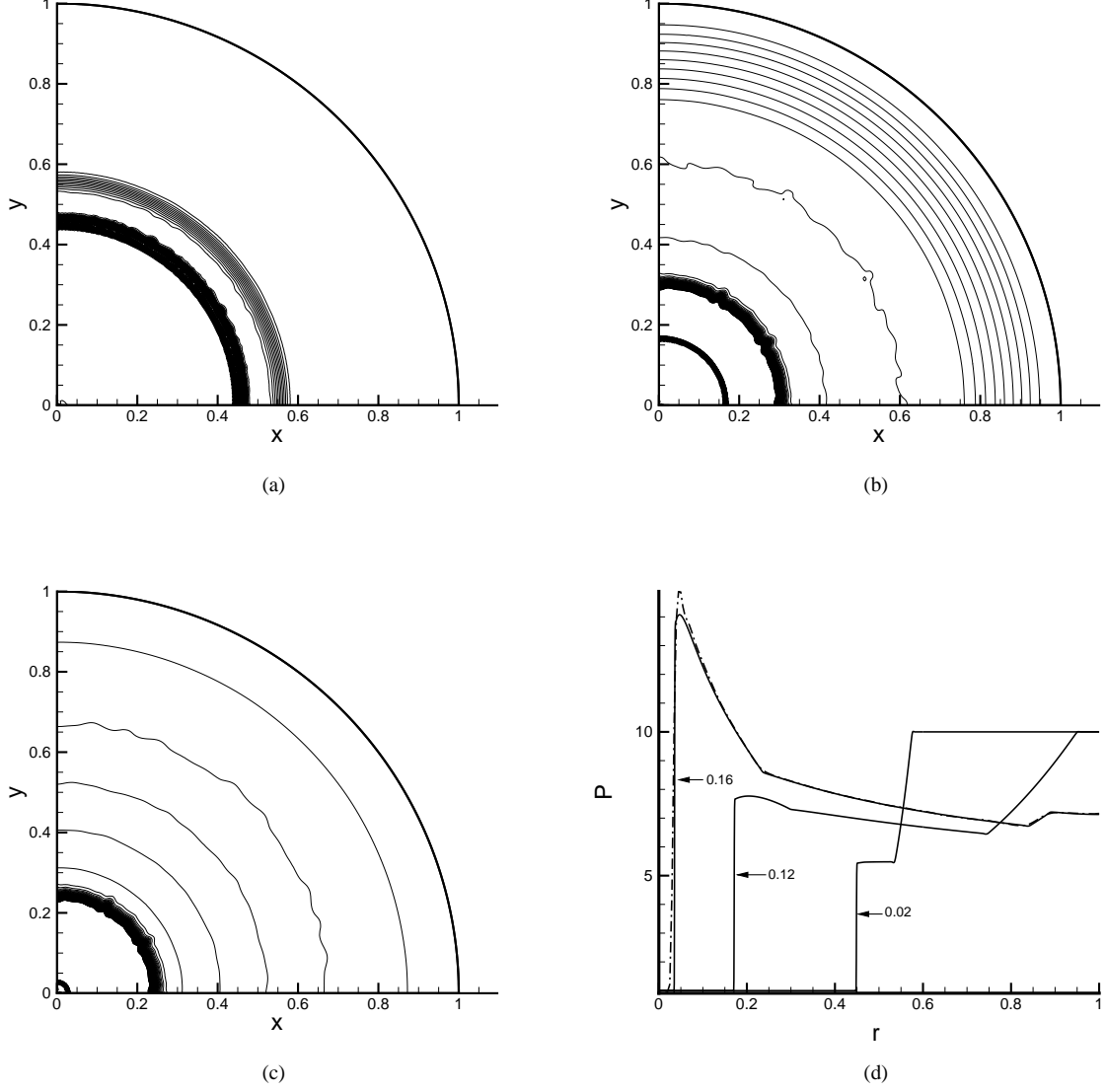


Figure 7: Density isoline for the cylindrical implosion problem: (a) $t = 0.02$; (b) $t = 0.12$; (c) $t = 0.16$. Each isoline corresponds to a density difference of $\Delta\rho/\rho_{ref} = 0.03$. (d) Pressure signal along the $y = 0$ axis at the same time levels: the solid line is the reference one-dimensional solutions, the dot-dashed line is the bidimensional solution.

Appendix A. Node-pair finite element for a scalar conservation law

In this appendix, the following two identities are demonstrated, namely

$$\sum_{k \in \mathcal{N}_i} \mathbf{f}_k^\varnothing \cdot \int_{\Omega_{ik}} R \varphi_k \nabla^\varnothing \varphi_i = \sum_{k \in \mathcal{N}_{i,\neq}} \left(\frac{\mathbf{f}_k^\varnothing + \mathbf{f}_i^\varnothing}{2} \cdot \boldsymbol{\eta}_{ik}^\varnothing - \frac{\mathbf{f}_k^\varnothing - \mathbf{f}_i^\varnothing}{2} \cdot \boldsymbol{\zeta}_{ik}^\varnothing \right) + \sum_{k \in \mathcal{N}_{i,\neq}} \frac{\mathbf{f}_k^\varnothing - \mathbf{f}_i^\varnothing}{2} \cdot \boldsymbol{\chi}_{ik}^\varnothing \quad (\text{A.1})$$

and

$$\sum_{k \in \mathcal{N}_i} \mathbf{f}_k^\varnothing \cdot \int_{\partial\Omega_{ik}^\varnothing} R \varphi_i \varphi_k \mathbf{n}^\varnothing = \sum_{k \in \mathcal{N}_{i,\neq}^\varnothing} (\mathbf{f}_k^\varnothing - \mathbf{f}_i^\varnothing) \cdot \boldsymbol{\chi}_{ik}^\varnothing - \mathbf{f}_i^\varnothing \cdot \boldsymbol{\xi}_i^\varnothing, \quad (\text{A.2})$$

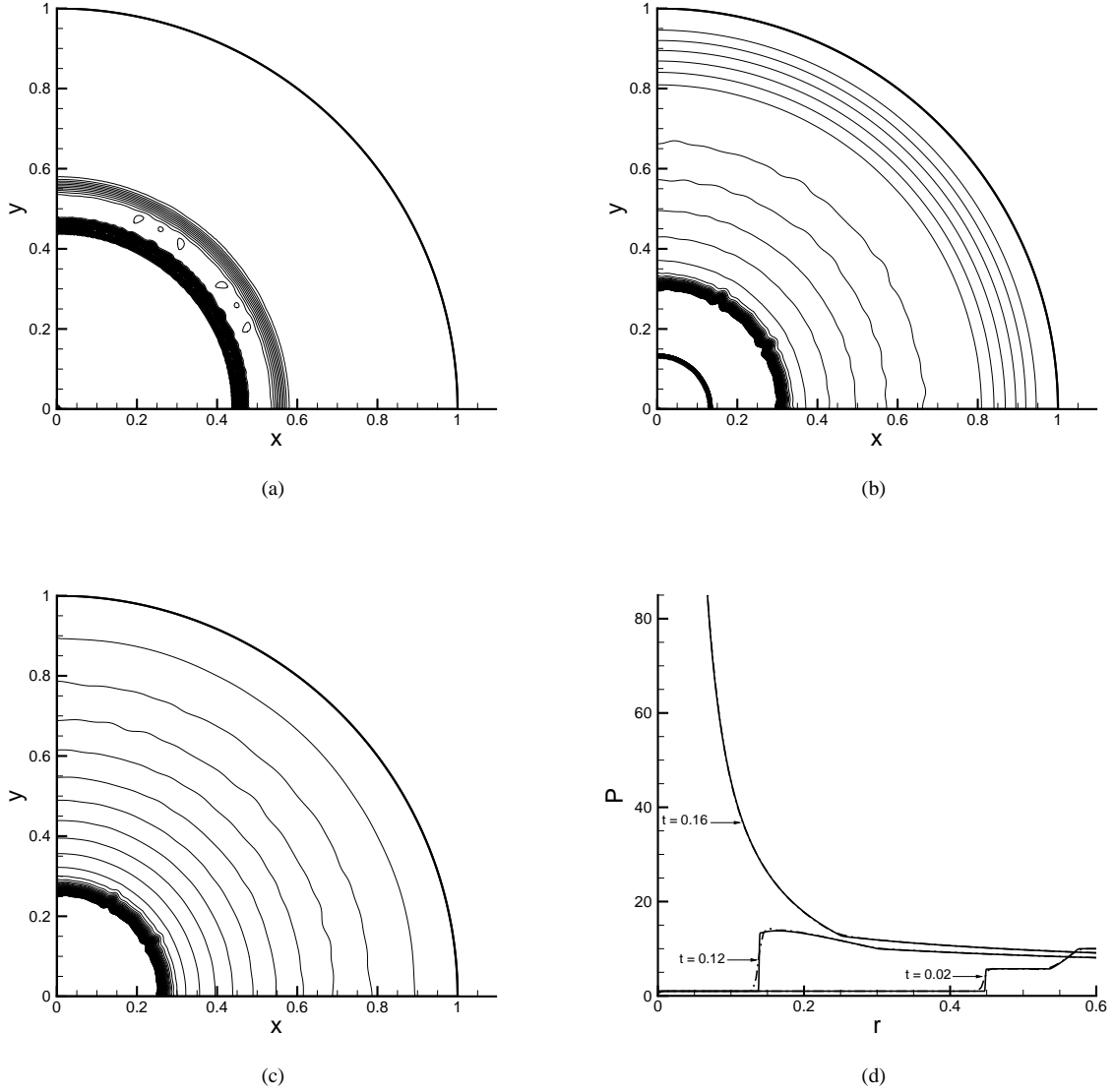


Figure 8: Density isoline for the spherical implosion problem: (a) $t = 0.02$; (b) $t = 0.12$; (c) $t = 0.16$. Each isoline corresponds to a density difference of $\Delta\rho/\rho_{ref} = 0.03$. (d) Pressure signal along the $y = 0$ axis at the same time levels: the solid line is the reference one-dimensional solutions, the dot-dashed line is the bidimensional solution.

which together allow to recast the discrete Bubnov-Galekin equation (6) in its node-pair counterpart (7).

The proof of the identity (A.1) is considered first. The integral on the left hand side of the Eq. (A.1) is assembled considering the contributions coming from each element e in the mesh, exploiting the local support property of the shape functions, as follows

$$\sum_{k \in \mathcal{N}_i} \mathbf{f}_k^\varnothing \cdot \int_{\Omega_{ik}} R\varphi_k \nabla^\varnothing \varphi_i = \sum_{e \in \mathcal{E}_i} \sum_{k \in \mathcal{N}^e} \mathbf{f}_k^\varnothing \cdot \int_{\Omega^e} R\varphi_k \nabla^\varnothing \varphi_i, \quad (\text{A.3})$$

where \mathcal{E}_i is the set of the elements having the node i in common and \mathcal{N}^e is the set of the nodes of element e . The first summation on the right-hand side is limited to the elements contained in the support Ω_i of node i , which are the only

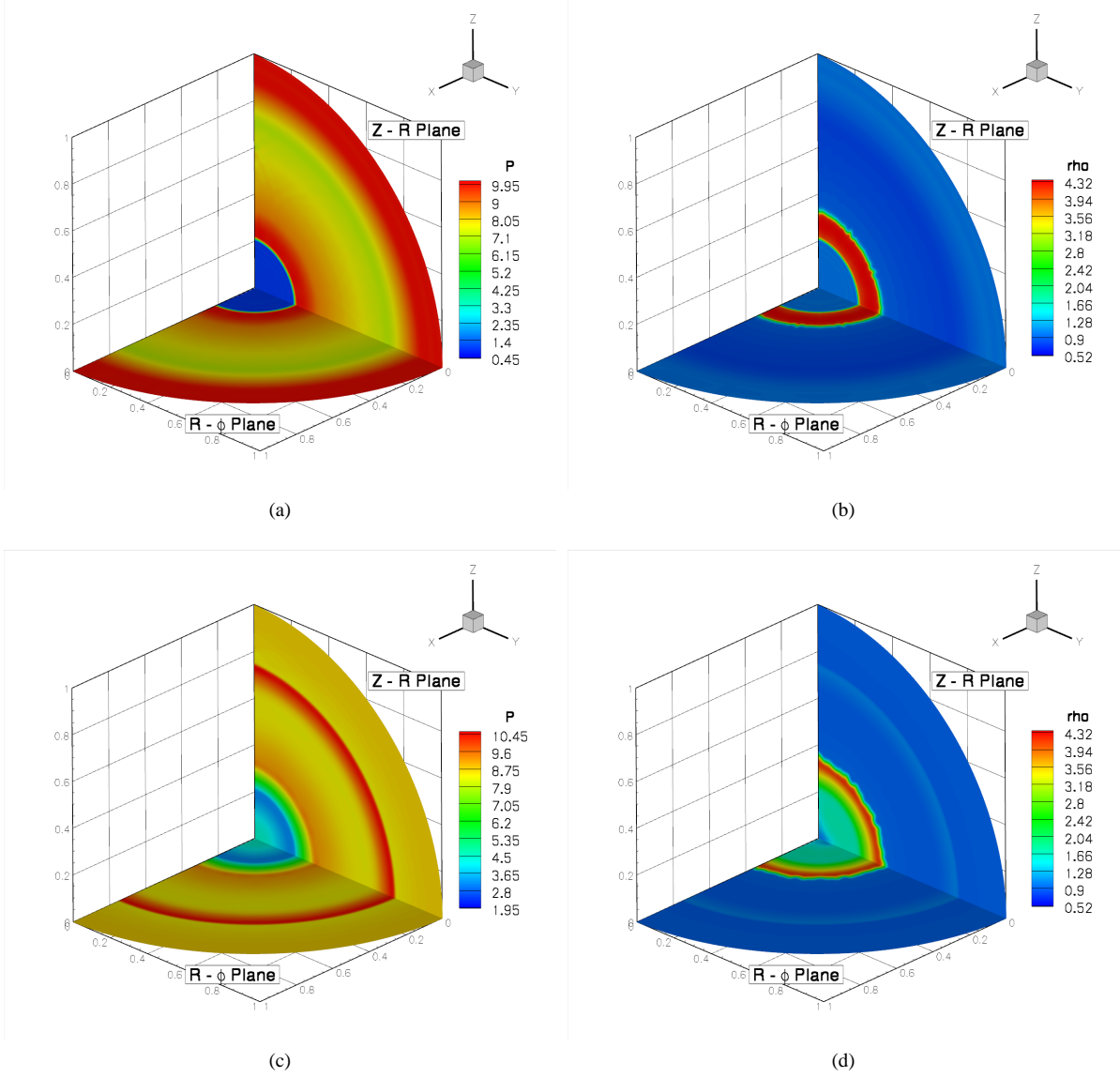


Figure 9: Pressure (a), (c) and density (b), (d) contours for the implosion problem at two different time levels: $t = 0.1$ first row, $t = 0.32$ second row. On the horizontal plane is represented the solution of the bidimensional spherical problem on the r - ϕ plane, while on the vertical plane is represented the solution of the cylindrical axisymmetric problem on the Z - R plane.

ones to give a nonzero contribution to integrals containing the function φ_i . Note that $\Omega_i = \bigcup_{e \in \mathcal{E}_i} \Omega^e$. Considering now the following identity from the Gauss theorem

$$\int_{\Omega^e} \nabla^\varnothing (R\varphi_i \varphi_k) d\Omega^\varnothing = \int_{\partial\Omega^e} R\varphi_i \varphi_k \mathbf{n}^\varnothing d\partial\Omega^\varnothing,$$

which allows to write

$$\int_{\Omega^e} R\varphi_k \nabla^\varnothing \varphi_i = - \int_{\Omega^e} R\varphi_i \nabla^\varnothing \varphi_k - \int_{\Omega^e} \varphi_i \varphi_k \hat{\mathbf{R}} + \int_{\partial\Omega^e} R\varphi_i \varphi_k \mathbf{n}^\varnothing. \quad (\text{A.4})$$

where $\hat{\mathbf{R}} = \nabla^\circ R$ is the unit vector in the radial direction. Thanks to the previous relation one deduces

$$\begin{aligned}
\int_{\Omega^e} R\varphi_k \nabla^\circ \varphi_i &= \frac{1}{2} \int_{\Omega^e} R\varphi_k \nabla^\circ \varphi_i + \frac{1}{2} \int_{\Omega^e} R\varphi_k \nabla^\circ \varphi_i \\
&= \frac{1}{2} \int_{\Omega^e} R\varphi_k \nabla^\circ \varphi_i + \frac{1}{2} \left(- \int_{\Omega^e} R\varphi_i \nabla^\circ \varphi_k - \int_{\Omega^e} \varphi_i \varphi_k \hat{\mathbf{R}} + \int_{\partial\Omega^e} R\varphi_i \varphi_k \mathbf{n}^\circ \right) \\
&= -\frac{1}{2} \boldsymbol{\eta}_{ik}^{e,\circ} - \frac{1}{2} \int_{\Omega^e} \varphi_i \varphi_k \hat{\mathbf{R}} + \frac{1}{2} \int_{\partial\Omega^e} R\varphi_i \varphi_k \mathbf{n}^\circ,
\end{aligned} \tag{A.5}$$

where in the last equality has been introduced the elemental contributions $\boldsymbol{\eta}_{ik}^{e,\circ}$ of the element e to the vector $\boldsymbol{\eta}_{ik}^\circ$

$$\boldsymbol{\eta}_{ik}^{e,\circ} \stackrel{\text{def}}{=} \int_{\Omega_{ik} \cap \Omega^e} R(\varphi_i \nabla^\circ \varphi_k - \varphi_k \nabla^\circ \varphi_i),$$

such that $\boldsymbol{\eta}_{ik}^\circ = \sum_{e \in (\mathcal{E}_i \cap \mathcal{E}_k)} \boldsymbol{\eta}_{ik}^{e,\circ}$. By the relation (A.5), the integral (A.3) becomes

$$\sum_{k \in N_i} \mathbf{f}_k^\circ \cdot \int_{\Omega_{ik}} R\varphi_k \nabla^\circ \varphi_i = - \sum_{e \in \mathcal{E}_i} \sum_{k \in N^e} \mathbf{f}_k^\circ \cdot \left(\frac{1}{2} \boldsymbol{\eta}_{ik}^{e,\circ} + \frac{1}{2} \int_{\Omega^e} \varphi_i \varphi_k - \frac{1}{2} \int_{\partial\Omega^e} R\varphi_i \varphi_k \mathbf{n}^\circ \right). \tag{A.6}$$

On the other hand, from the Eq. (A.5) follows also that

$$\boldsymbol{\eta}_{ik}^{e,\circ} = -2 \int_{\Omega^e} R\varphi_k \nabla^\circ \varphi_i - \int_{\Omega^e} \varphi_i \varphi_k \hat{\mathbf{R}} + \int_{\partial\Omega^e} R\varphi_i \varphi_k \mathbf{n}^\circ,$$

which can be recast, using the equation (A.4), as

$$\boldsymbol{\eta}_{ik}^{e,\circ} = 2 \int_{\Omega^e} R\varphi_i \nabla^\circ \varphi_k + \int_{\Omega^e} \varphi_i \varphi_k \hat{\mathbf{R}} - \int_{\partial\Omega^e} R\varphi_i \varphi_k \mathbf{n}^\circ.$$

Summing up the last relation for all the nodes k belonging to the element Ω^e and using the fact that $\sum_{k \in N^e} \nabla^\circ \varphi_k(\mathbf{x}^\circ) = \mathbf{0}$, $\forall \mathbf{x}^\circ \in \Omega^e$, one obtains

$$\sum_{k \in N^e} \left(\boldsymbol{\eta}_{ik}^{e,\circ} - \int_{\Omega^e} \varphi_i \varphi_k \hat{\mathbf{R}} + \int_{\partial\Omega^e} R\varphi_i \varphi_k \mathbf{n}^\circ \right) = \mathbf{0}. \tag{A.7}$$

Summing up the previous relation for all the elements belonging to \mathcal{E}_i and multiplying by the vector \mathbf{f}_i° , follows that

$$\sum_{e \in \mathcal{E}_i} \sum_{k \in N^e} \mathbf{f}_i^\circ \cdot \left(\boldsymbol{\eta}_{ik}^{e,\circ} - \int_{\Omega^e} \varphi_i \varphi_k \hat{\mathbf{R}} + \int_{\partial\Omega^e} R\varphi_i \varphi_k \mathbf{n}^\circ \right) = \mathbf{0}.$$

Multiplying this relation by 1/2 and adding it to the right hand side of (A.6) one has

$$\begin{aligned}
\sum_{k \in N_i} \mathbf{f}_k^\circ \cdot \int_{\Omega_{ik}} R\varphi_k \nabla^\circ \varphi_i &= - \sum_{e \in \mathcal{E}_i} \sum_{k \in N^e} \left(\frac{\mathbf{f}_k^\circ + \mathbf{f}_i^\circ}{2} \cdot \boldsymbol{\eta}_{ik}^{e,\circ} + \frac{\mathbf{f}_k^\circ - \mathbf{f}_i^\circ}{2} \cdot \int_{\Omega^e} \varphi_i \varphi_k \hat{\mathbf{R}} \right) \\
&\quad + \sum_{e \in \mathcal{E}_i} \sum_{k \in N^e} \frac{\mathbf{f}_k^\circ - \mathbf{f}_i^\circ}{2} \cdot \int_{\partial\Omega^e} R\varphi_i \varphi_k \mathbf{n}^\circ.
\end{aligned}$$

By recalling that $\boldsymbol{\eta}_{ik}^{e,\circ} = \mathbf{0}$ for $e \notin (\mathcal{E}_i \cap \mathcal{E}_k)$, that $\boldsymbol{\eta}_{ik}^\circ = \sum_{e \in (\mathcal{E}_i \cap \mathcal{E}_k)} \boldsymbol{\eta}_{ik}^{e,\circ}$ and that $\boldsymbol{\eta}_{ii}^\circ = \mathbf{0}$, the right hand side of the last equation can be written as

$$\begin{aligned}
\sum_{k \in N_i} \mathbf{f}_k^\circ \cdot \int_{\Omega_{ik}} R\varphi_k \nabla^\circ \varphi_i &= - \sum_{k \in N_{i,\neq}} \left(\frac{\mathbf{f}_k^\circ + \mathbf{f}_i^\circ}{2} \cdot \boldsymbol{\eta}_{ik}^\circ + \frac{\mathbf{f}_k^\circ - \mathbf{f}_i^\circ}{2} \cdot \boldsymbol{\zeta}_{ik}^\circ \right) \\
&\quad + \sum_{k \in N_{i,\neq}^\circ} \frac{\mathbf{f}_k^\circ - \mathbf{f}_i^\circ}{2} \cdot \int_{\partial\Omega_{ik}^\circ} R\varphi_i \varphi_k \mathbf{n}^\circ,
\end{aligned}$$

that is the relation (A.1).

Considering now the proof of the identity (A.2), in the left hand side of (A.2) the contribute of the node i is put into evidence, namely

$$\sum_{k \in \mathcal{N}_i^\partial} \mathbf{f}_k^\partial \cdot \int_{\partial\Omega_{ik}^\partial} \mathbf{R}\varphi_i\varphi_k \mathbf{n}^\partial = \sum_{k \in \mathcal{N}_{i,\neq}^\partial} \mathbf{f}_k^\partial \cdot \int_{\partial\Omega_{ik}^\partial} \mathbf{R}\varphi_i\varphi_k \mathbf{n}^\partial + \mathbf{f}_i^\partial \cdot \int_{\partial\Omega_{ik}^\partial} \mathbf{R}\varphi_i\varphi_i \mathbf{n}^\partial.$$

The quantity

$$\sum_{k \in \mathcal{N}_{i,\neq}^\partial} \mathbf{f}_i^\partial \cdot \int_{\partial\Omega_{ik}^\partial} \mathbf{R}\varphi_i\varphi_k \mathbf{n}^\partial,$$

is now added and subtracted from the right hand side to obtain

$$\sum_{k \in \mathcal{N}_i^\partial} \mathbf{f}_k^\partial \cdot \int_{\partial\Omega_{ik}^\partial} \mathbf{R}\varphi_i\varphi_k \mathbf{n}^\partial = \sum_{k \in \mathcal{N}_{i,\neq}^\partial} (\mathbf{f}_k^\partial - \mathbf{f}_i^\partial) \cdot \int_{\partial\Omega_{ik}^\partial} \mathbf{R}\varphi_i\varphi_k \mathbf{n}^\partial + \mathbf{f}_i^\partial \cdot \sum_{k \in \mathcal{N}_i^\partial} \int_{\partial\Omega_{ik}^\partial} \mathbf{R}\varphi_i\varphi_k \mathbf{n}^\partial.$$

By recalling that $\sum_{k \in \mathcal{N}_e} \varphi_k(\mathbf{x}^\partial) = 1, \mathbf{x}^\partial \in \Omega^e, \forall e \in \mathcal{E}$, one has

$$\begin{aligned} \sum_{k \in \mathcal{N}_i^\partial} \mathbf{f}_k^\partial \cdot \int_{\partial\Omega_{ik}^\partial} \mathbf{R}\varphi_i\varphi_k \mathbf{n}^\partial &= \sum_{k \in \mathcal{N}_{i,\neq}^\partial} (\mathbf{f}_k^\partial - \mathbf{f}_i^\partial) \cdot \int_{\partial\Omega_{ik}^\partial} \mathbf{R}\varphi_i\varphi_k \mathbf{n}^\partial + \mathbf{f}_i^\partial \cdot \int_{\partial\Omega_i^\partial} \mathbf{R}\varphi_i \mathbf{n}^\partial \\ &= \sum_{k \in \mathcal{N}_{i,\neq}^\partial} (\mathbf{f}_k^\partial - \mathbf{f}_i^\partial) \cdot \boldsymbol{\chi}_{ik}^\partial + \mathbf{f}_i^\partial \cdot \boldsymbol{\xi}_i^\partial, \end{aligned}$$

which is the relation (A.2). Using the relations (A.1), (A.2) is possible to write (6) as follow

$$\begin{aligned} \sum_{k \in \mathcal{N}_i} M_{ik}^\partial \frac{du_k}{dt} &= - \sum_{k \in \mathcal{N}_{i,\neq}} \left(\frac{\mathbf{f}_k^\partial + \mathbf{f}_i^\partial}{2} \cdot \boldsymbol{\eta}_{ik}^\partial + \frac{\mathbf{f}_k^\partial - \mathbf{f}_i^\partial}{2} \cdot \boldsymbol{\zeta}_{ik}^\partial \right) + \sum_{k \in \mathcal{N}_i} \mathbf{f}_k^\partial \cdot \int_{\Omega_{ik}} \varphi_i\varphi_k \hat{\mathbf{R}} \\ &\quad - \sum_{k \in \mathcal{N}_{i,\neq}^\partial} \frac{\mathbf{f}_k^\partial - \mathbf{f}_i^\partial}{2} \cdot \boldsymbol{\chi}_{ik}^\partial - \mathbf{f}_i^\partial \cdot \boldsymbol{\xi}_i^\partial, \end{aligned} \tag{A.8}$$

with the metric quantities defined in the subsection 4.1. In the previous relation is necessary to write in node-pair form also the second term on the right hand side. By recalling that

$$\sum_{k \in \mathcal{N}_i} \mathbf{f}_k^\partial \cdot \int_{\Omega_{ik}} \varphi_i\varphi_k \hat{\mathbf{R}} = \sum_{k \in \mathcal{N}_{i,\neq}} \mathbf{f}_k^\partial \cdot \int_{\Omega_{ik}} \varphi_i\varphi_k \hat{\mathbf{R}} + \mathbf{f}_i^\partial \cdot \int_{\Omega_{ik}} \varphi_i\varphi_k \hat{\mathbf{R}},$$

by adding and subtracting to the previous relation the following quantity

$$\sum_{k \in \mathcal{N}_{i,\neq}} \mathbf{f}_i^\partial \cdot \int_{\Omega_{ik}} \varphi_i\varphi_k \hat{\mathbf{R}},$$

one has

$$\begin{aligned} \sum_{k \in \mathcal{N}_i} \mathbf{f}_k^\partial \cdot \int_{\Omega_{ik}} \varphi_i\varphi_k \hat{\mathbf{R}} &= \sum_{k \in \mathcal{N}_{i,\neq}} (\mathbf{f}_k^\partial - \mathbf{f}_i^\partial) \cdot \int_{\Omega_{ik}} \varphi_i\varphi_k \hat{\mathbf{R}} + \sum_{k \in \mathcal{N}_i} \mathbf{f}_i^\partial \cdot \int_{\Omega_{ik}} \varphi_i\varphi_k \hat{\mathbf{R}} \\ &= \sum_{k \in \mathcal{N}_{i,\neq}} (\mathbf{f}_k^\partial - \mathbf{f}_i^\partial) \cdot \int_{\Omega_{ik}} \varphi_i\varphi_k \hat{\mathbf{R}} + \mathbf{f}_i^\partial \cdot \int_{\Omega_{ik}} \varphi_i \hat{\mathbf{R}} \\ &= \sum_{k \in \mathcal{N}_{i,\neq}} (\mathbf{f}_k^\partial - \mathbf{f}_i^\partial) \cdot \int_{\Omega_{ik}} \varphi_i\varphi_k \hat{\mathbf{R}} + \mathbf{f}_i^\partial \cdot \tilde{\mathbf{L}}_i^\partial. \end{aligned} \tag{A.9}$$

by substituting this relation into the (A.8) one has the node-pair FE discretization of the scalar equation (2)

$$L_i^\varnothing \frac{du_i}{dt} = - \sum_{k \in N_{i,\neq}} \left(\frac{f_k^\varnothing + f_i^\varnothing}{2} \cdot \eta_{ik}^\varnothing - \frac{f_k^\varnothing - f_i^\varnothing}{2} \cdot \zeta_{ik}^\varnothing \right) + f_i^\varnothing \cdot \widehat{L}_i^\varnothing - \sum_{k \in N_{i,\neq}^\beta} \frac{f_k^\varnothing - f_i^\varnothing}{2} \cdot \chi_{ik}^\varnothing - f_i^\varnothing \cdot \xi_i^\varnothing, \quad (\text{A.10})$$

where the mass matrix has been lumped

$$\sum_{k \in N_i} M_{ik}^\varnothing \frac{du_i}{dt} \simeq L_i^\varnothing \frac{du_i}{dt},$$

with $L_i^\varnothing = \sum_{k \in N_i} M_{ik}^\varnothing$.

References

- [1] L. I. Sedov, *Similarity and dimensional methods in mechanics*, Academic Press, 1959.
- [2] L. Fezou, B. Stoufflet, A class of implicit upwind schemes for Euler simulations with unstructured meshes, *J. Comput. Phys.* 84 (1989) 174 – 206.
- [3] L. Z. H. B. Chen, E. Panarella, Stability of imploding spherical shock waves, *Journal of Fusion Energy* 14 (1995) 389–392.
- [4] V. Selmin, The node-centred finite volume approach: bridge between finite differences and finite elements, *Comp. Meth. Appl. Mech. Engng.* 102 (1993) 107 – 138.
- [5] V. Selmin, L. Formaggia, Unified construction of finite element and finite volume discretizations for compressible flows, *Int. J. Numer. Meth. Eng.* 39 (1996) 1 – 32.
- [6] A. Guardone, L. Vigeveno, Finite element/volume solution to axisymmetric conservation laws, *J. Comput. Phys.* 224 (2) (2007) 489 – 518.
- [7] D. De Santis, G. Geraci, A. Guardone, Equivalence conditions for finite volume/element discretizations in cylindrical coordinates, V European Conference on Computational Fluid Dynamics ECCOMAS CFD 2010, 2010.
- [8] A. Guardone, D. De Santis, G. Geraci, M. Pasta, On the relation between finite element and finite volume schemes for compressible flows with cylindrical and spherical symmetry, *J. Comput. Phys.* 230 (2010) 680–694.
- [9] J. Donea, A. Huerta, *Finite Element Methods for Flow Problems*, Wiley, New York, 2002.
- [10] R. J. LeVeque, *Finite volume methods for conservation laws and hyperbolic systems*, Cambridge University Press, 2002.
- [11] D. De Santis, G. Geraci, A. Guardone, Finite volume and finite element schemes for the euler equations in spherical coordinates. (under review), *Math. Comput. Simulat.*
- [12] A. Harten, J. M. Hyman, Self adjusting grid methods for one-dimensional hyperbolic conservation laws, *J. Comput. Phys.* 50 (1983) 253–269.
- [13] B. van Leer, Towards the ultimate conservative difference scheme II. Monotonicity and conservation combined in a second order scheme, *J. Comput. Phys.* 14 (1974) 361 – 370.
- [14] V. Venkatakrishnan, D. J. Mavriplis, Implicit method for the computation of unsteady flows on unstructured grids, *Tech. rep.* (1995).
- [15] G. Guderley, Powerful spherical and cylindrical compression shocks in the neighbourhood of the centre and of the cylinder axis, *Luftfahrt-forschung* 19 (1942) 302–312.